ChemComm

COMMUNICATION

View Article Online
View Journal | View Issue

Cite this: *Chem. Commun.*, 2018, **54**, 2122

Received 4th December 2017,
Accepted 26th January 2018

DOI: 10.1039/c7cc09240g

rsc.li/chemcomm

Synthesis and structure determination *via* ultra-fast electron diffraction of the new microporous zeolitic germanosilicate ITQ-62†

Lindiane Bieseki,[ab] Raquel Simancas,[a] Jose L. Jordá,[a] Pablo J. Bereciartua,‡[a] Ángel Cantín,[a] Jorge Simancas,[a] Sibele B. Pergher,[b] Susana Valencia,[a] Fernando Rey *[a] and Avelino Corma *[a]

Here, we present the synthesis and structure determination of the new zeolite ITQ-62. Its structure was determined *via* ultra-fast electron diffraction tomography and refined using powder XRD data of the calcined material. This new zeolite contains a tridirectional channel system of highly distorted 8-rings, as well as a monodirectional 12-ring channel system.

Zeolites are usually described as crystalline microporous silica-based materials. In many cases, it is possible to replace a part of the silica atoms by other elements, such as Al, Ti, B, or Ge, among others, obtaining aluminosilicates, titanosilicates, borosilicates or germanosilicates. The isomorphic incorporation of heteroatoms other than silicon confers to the resulting materials different catalytic properties, which can be nicely tailored for a particular catalytic reaction. Therefore, the properties and potential applications of zeolites strongly depend on their chemical composition, but are equally dependent on the size and spatial distribution of their channel systems.

The driving force for obtaining new zeolites with novel channel systems is the clever selection of organic structure directing agents (OSDA). Indeed, from the earlier work of Barrer[1,2] and Kerr[3] reporting the use of tetraalkylammonium cations as OSDA for decreasing the Al content in zeolites to the very sophisticated organic synthesis strategies pursued for obtaining very complex OSDA,[4–18] the range of zeolites available as excellent acid catalysts useful for many industrial applications has been extraordinarily expanded.[19–24]

Recently, a new zeolite named ITQ-55 has been reported. This was obtained as a pure silica material and presents an 8-ring channel system that has been found to possess great potential for gas separations.[25]

The OSDA used for the synthesis of the new material ITQ-62 was the same diammonium cation (N^2,N^2,N^2,N^5,N^5,N^5,3*a*,6*a*-octamethyloctahydropentalene-2,5-diammonium) employed for zeolite ITQ-55.

Exploring the possibilities of this particular OSDA, we found that using concentrated synthesis gels in the presence of fluoride anions and germanium led to the formation of a new zeolite, named ITQ-62. Both F^- and Ge are two well-known strong inorganic structure directing agents that induce the formation of zeolites containing double four-ring units (D4R).[26–41]

The preparation of the OSDA and the synthesis conditions are shown in the ESI† (Table S1). Under some of these conditions, the new zeolitic phase ITQ-62 was obtained as an almost pure phase with an impurity content less than 3%.

The chemical analysis of the resulting material shows a Si/Ge ratio incorporated in the zeolitic material (3.0), which is much lower than that used in its synthesis gel (5.2). This indicates that some of the Si is not incorporated to the solid. On the other hand, the C/N ratio and the ^{13}C-CP-MAS-NMR spectrum of the occluded OSDA in ITQ-62 (see ESI†) indicate that the diammonium cation remains intact during the zeolite formation.

The new zeolite ITQ-62 is structurally stable after removing the OSDA by thermal treatment at 923 K in dry air. Volumetric adsorption of N_2 shows a microporous solid of 313 $m^2\ g^{-1}$ and 0.19 $cm^3\ g^{-1}$ BET surface area and *t*-plot micropore volume, respectively. The Ar adsorption isotherm shows that the averaged micropore diameter is 6.2 Å according to the Horvath–Kawazoe formalism.

The laboratory X-ray diffraction pattern of the calcined sample was obtained in a PANalytical X'Pert PRO diffractometer with Bragg–Brentano geometry, using CuKα radiation, as described in the ESI.† The sample was *in situ* calcined at 923 K for 5 hours in an Anton Parr XRK-900 reaction chamber attached to the

[a] *Instituto de Tecnología Química (UPV-CSIC), Universitat Politècnica de València – Consejo Superior de Investigaciones Científicas, Av. de los Naranjos s/n, 46022 Valencia, Spain. E-mail: frey@itq.upv.es*

[b] *Universidade Federal do Rio Grande do Norte, Natal, RN, Brazil*

† Electronic supplementary information (ESI) available: Synthesis and characterization procedures, Fig. S1–S8, Tables S1–S3 and crystallographic information. Further details of the crystal structure may be obtained from ICSD at FIZ Karlsruhe on quoting the deposition number CSD-433848. See DOI: 10.1039/c7cc09240g

‡ Present address: Deutsches Elektronen-Synchrotron (DESY), Notkestraße 85, 22607 Hamburg, Germany.

diffractometer under a continuous flow of dry air to decompose the occluded OSDA and ensure the complete dryness of the sample before the measurement. The pattern was indexed using the program TREOR,[42] obtaining a possible orthorhombic unit cell with a = 21.068 Å, b = 17.254 Å, and c = 7.554 Å. The systematic extinctions suggested as the most probable extinction symbol C – – –, corresponding to space groups $C222$, $C2mm$, $Cm2m$, $Cmm2$ or $Cmmm$.

The structure resolution was attempted using two independent methods.

In the first method, the OSDA-containing sample was measured *via* ultra-fast electron diffraction tomography (EDT) in a JEOL 2100F microscope operating at 200 kV and using a GATAN Orius SC600A CCD camera. A NanoMEGAS-Digistar P1000 device, attached to the microscope, is also employed to control the precession of the electron beam. This method, recently described, allows collecting large sets of electron diffraction tomography data in just half a minute.[25,43] Performing the data collection in such a short time enables obtaining good datasets even for highly beam-sensitive samples such as germanosilicate zeolites, as the measurement is completed before the beam damage precludes data acquisition due to the complete amorphization of the structure.

The dataset obtained *via* EDT for the OSDA-containing material was analysed using the program ADT3D.[44] After combining the diffraction patterns corresponding to the different orientations, the Bragg peak distribution can be indexed with a unit cell very similar to that of the calcined sample, with a = 20.61 Å, b = 17.92 Å, and c = 7.62 Å. This result strongly suggests that during the calcination no important variations of the structure occur. Also, the systematic extinctions are compatible with the space groups previously found. The obtained integrated intensities were introduced into the software FOCUS,[45] leading to the crystal structure solution using the space group with the highest symmetry (*Cmmm*). After determining the positions of the four independent T atoms, the positions of the ten bridging O-atoms were calculated using the program KRIBER,[46] and the coordinates of all the atoms were optimized geometrically with DLS-76.[47]

Simultaneously, for the second method, one sample of ITQ-62 was calcined at 923 K, transferred to a glass capillary and sealed. Then, the XRPD pattern was measured at the beamline MSPD of the Spanish Synchrotron Light Source ALBA using a high resolution setup.[48,49] The orthorhombic unit cell parameters obtained using the laboratory and EDT data were confirmed to be correct. Integrated intensities were extracted using the program FULLPROF,[50] and the crystal structure was solved again with FOCUS using the same procedure followed for the EDT data, obtaining an identical solution.

Finally, the structure was validated by a Rietveld refinement of the XRPD data using FULLPROF. Due to the presence of the peaks of the impurity phase in the synchrotron data, a new sample with a lower content of impurities was synthesised and measured using the laboratory diffractometer. These data were used for the refinement. The regions of the diffraction pattern containing the strongest peaks of the impurity were excluded

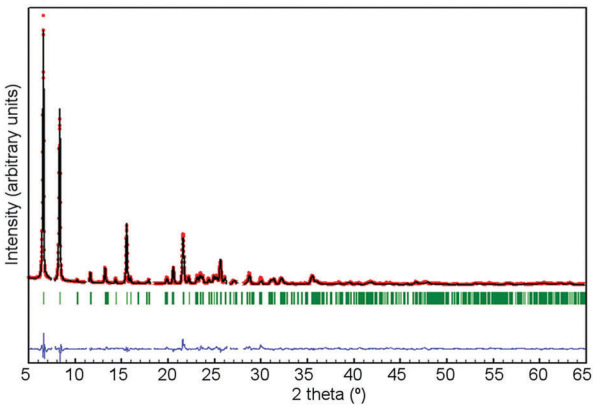

Fig. 1 Rietveld refinement of the X-ray diffraction pattern of calcined ITQ-62. Red data points show the observed XRPD pattern; the black line along these points is the calculated XRPD pattern, with the difference profile at the bottom in blue. The green vertical ticks give the positions of the Bragg reflections. Residual values: R_{wp} = 0.153, R_{exp} = 0.047, R_B = 0.069 and R_F = 0.072. Wavelength corresponds to Cu Kα.

during the refinement (see ESI†). As the T–O9–T angle is constrained by symmetry to be 180°, the atom O9 was shifted out of its special position (1/4, 1/4, 1/2) to a general one, and its occupancy was accordingly reduced. After the refinement process, the final coordinates obtained for this atom clearly indicate that it is located at another special position (1/4, 1/4, z), implying suitable values for the T–O9–T angle. After the refinement, the residual values were R_{wp} = 0.153, R_{exp} = 0.047, R_B = 0.069 and R_F = 0.072. The relatively high value of R_{wp} could be explained by the presence of the less intense diffraction peaks of the impurity, which were not completely removed during the refinement. The refined XRPD pattern is shown in Fig. 1.

The projections of the structure along the main crystallographic axis are shown in Fig. 2. As it can be seen, the zeolite ITQ-62 presents a tridirectional channel system with 8-ring apertures, as well as a monodirectional channel system with 12-ring apertures. The pore openings of the channels along the a and b axes are very elongated 8R, with 3.9 Å × 2.4 Å and 4.9 Å × 2.1 Å, respectively. While the first 8R pore window

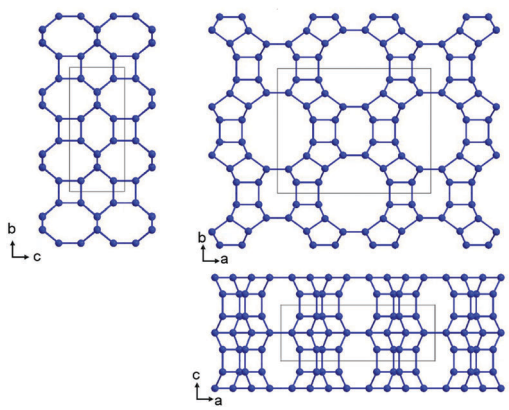

Fig. 2 Structure of the zeolite ITQ-62. View along the main crystallographic axes. Oxygen atoms have been removed for clarity.

(3.9 × 2.4 Å) is almost flat and inclined, the second one (4.9 Å × 2.1 Å) is boat shaped. Along the *c* axis, there are two different, parallel channels systems with different pore apertures. One channel has boat shaped, elongated 8-ring 5.1 Å × 1.5 Å openings, while the second channel running along *c* has almost circular boat-shaped 12-ring openings of 6.8 Å × 6.1 Å aperture. The shape of the pore openings can be seen in the ESI† (Fig. S8). The elongated 8*R* channels along *c* are connected with the channels along *b*, while the circular 12*R* ones intercross with the channels along *b* and also with pairs of channels along *a*. Thus, depending on the size of the selected target molecule, zeolite ITQ-62 could perform as a tri-, bi- or monodirectional molecular sieve.

The structure of ITQ-62 can be described with three main building units: $[4^6]$ or D4R, $[4^25^46^2]$ or mtw, and $[4^45^48^2]$ (Fig. 3a). The units D4R and mtw are connected alternately forming linear chains along the *c* axis by sharing a 4*R* face (Fig. 3b). Then, the chains stack zigzagging along *b*, forming layers in the *bc* plane by sharing a side of the mtw units as well as generating the $[4^45^48^2]$ units (Fig. 3c). Finally, the layers stack along *a* with a displacement of *b*/2, connecting through one corner of each mtw units, giving rise to the complete tridimensional structure (Fig. 3d and e).

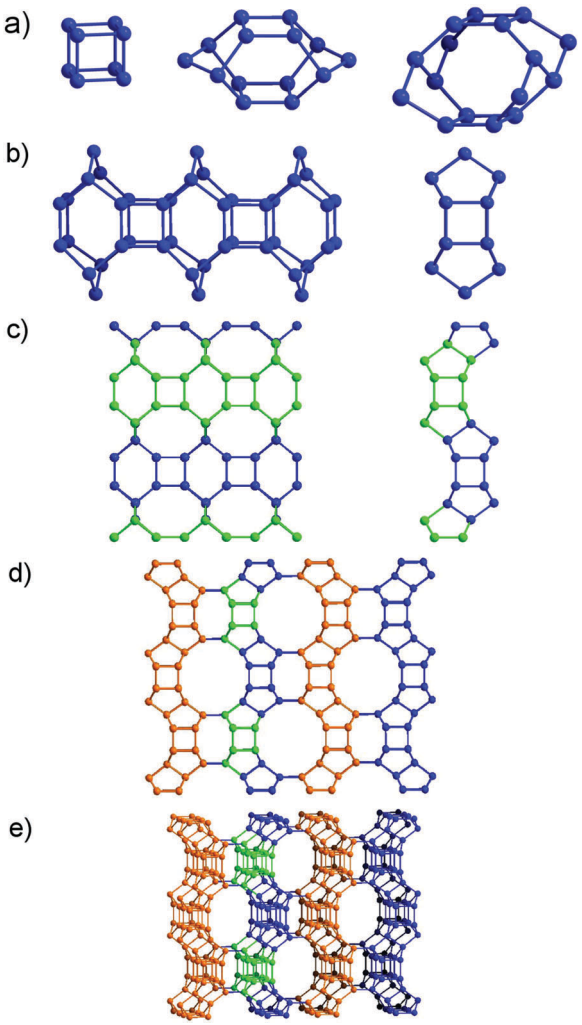

Fig. 3 Structure of ITQ-62: (a) main building units: D4R, mtw, and $[4^45^48^2]$; (b) connection of D4R and mtw forming chains along *c* (lateral and frontal views); (c) connection of the chains forming layers in the *bc* plane (lateral and frontal views); (d) stacking and connection of the layers forming the complete 3D structure; and (e) perspective view of zeolite ITQ-62. (Oxygen atoms omitted for clarity.)

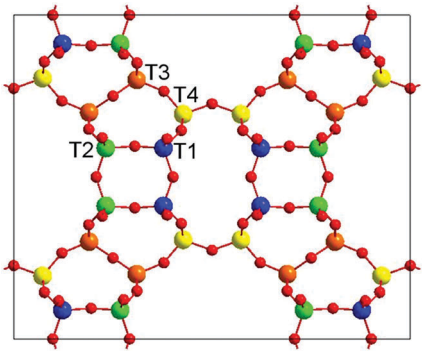

Fig. 4 Location of the Ge atoms in the ITQ-62 structure. T1: 34 atomic % Ge, T2: 29%, T3: 0%, T4: 12%.

Also, in order to determine the distribution of Ge in the different sites, the occupancies of the T-sites were refined as mixed Si/Ge positions. The refinement shows a preferential occupation of Ge in certain T sites. T1 and T2, corresponding to the D4R units, contain the highest Ge contents (34 and 29 atomic %, respectively), while T3 remains as purely siliceous and T4, which connects the *bc* layers, contains 12% Ge (Fig. 4). This is in good agreement with the results found for other germanium-containing zeolites presenting D4R units in their structures.[31–41]

In conclusion, a new zeolite, named ITQ-62, has been synthesized using the same OSDA previously described for the synthesis of zeolite ITQ-55. Its structure has been solved using both synchrotron PXRD data for the calcined sample and EDT for the OSDA-containing one. Ultra-fast EDT has been proved to be an extremely useful tool for the structure solution of materials with low stability. Moreover, it can be applied also to samples containing impurities, since the selection of a suitable isolated crystal allows obtaining data from a single phase. The new zeolite ITQ-62 presents a complex pore system, potentially allowing it to behave as a mono-, bi- or tridirectional molecular sieve depending on the size of molecules that travel along its channel system.

The authors gratefully acknowledge financial support from the Spanish Government (MAT2015-71842-P and MAT2015-71261-R MINECO/FEDER and Severo Ochoa SEV-2016-0683). The authors thank ALBA Light Source for beam allocation at the beamline MSPD, and specially thank the Electron Microscopy Service of the Universitat Politècnica de València. Finally, the authors thank Dr Alejandro Vidal and Dr Teresa Blasco for helping in the NMR data discussion.

Conflicts of interest

There are no conflicts to declare.

Notes and references

1 R. M. Barrer and P. J. Denny, *J. Chem. Soc.*, 1961, 971–982.
2 R. M. Barrer, P. J. Denny and E. M. Flanigen, *US Pat.*, 3306922, 1967.
3 G. T. Kerr, *Inorg. Chem.*, 1966, **5**, 1537–1539.
4 R. F. Lobo, S. I. Zones and M. E. Davis, *J. Inclusion Phenom. Mol. Recognit. Chem.*, 1995, **21**, 47–78.
5 A. W. Burton and S. I. Zones, *Stud. Surf. Sci. Catal.*, 2007, **168**, 137–179.
6 M. E. Davis and S. I. Zones, *Chem. Ind.*, 1997, **69**, 1–34.
7 S. I. Zones, Y. Nakagawa, G. S. Lee, C. Y. Chen and L. T. Yuen, *Microporous Mesoporous Mater.*, 1998, **21**(4–6), 199–211.
8 A. W. Burton, S. I. Zones and S. Elomari, *Curr. Opin. Colloid Interface Sci.*, 2005, **10**(5–6), 211–219.
9 M. Moliner, F. Rey and A. Corma, *Angew. Chem., Int. Ed.*, 2013, **52**, 13880–19889.
10 G. T. Park, D. Jo, N. H. Ahn, J. Cho and S. B. Hong, *Inorg. Chem.*, 2017, **56**(14), 8504–8512.
11 D. L. Dorset, K. G. Strohmaier, C. E. Kliewer, A. Corma, M. J. Dıaz-Cabañas, F. Rey and C. J. Gilmore, *Chem. Mater.*, 2008, **20**, 5325–5331.
12 D. L. Dorset, G. J. Kennedy, K. G. Strohmaier, M. J. Diaz-Cabañas, F. Rey and A. Corma, *J. Am. Chem. Soc.*, 2006, **128**, 8862–8867.
13 D. Jo, T. Ryu, G. T. Park, P. S. Kim, Ch. H. Kim, I.-S. Nam and S. B. Hong, *ACS Catal.*, 2016, **6**(4), 2443–2447.
14 M. A. Miller, J. G. Moscoso, S. C. Koster, M. G. Gatter and G. J. Lewis, *Stud. Surf. Sci. Catal.*, 2007, **170A**, 347–354.
15 R. Simancas, J. L. Jorda, F. Rey, A. Corma, A. Cantín, I. Peral and C. Popescu, *J. Am. Chem. Soc.*, 2014, **136**, 3342–3345.
16 R. Simancas, D. Dari, N. Velamazán, M. T. Navarro, A. Cantín, J. L. Jordá, G. Sastre, A. Corma and F. Rey, *Science*, 2010, **330**, 1219–1222.
17 R. Martínez-Franco, M. Moliner, Y. Yun, J. Sun, W. Wan, X. Zou and A. Corma, *Proc. Natl. Acad. Sci. U. S. A.*, 2013, **110**, 3749–3754.
18 M. Choi, K. Na, J. Kim, Y. Sakamoto, O. Terasaki and R. Ryoo, *Nature*, 2009, **461**, 246–249.
19 S. I. Zones and M. E. Davis, *Curr. Opin. Solid State Mater. Sci.*, 1996, **1**(1), 107–117.
20 G. Bellussi, A. Carati and R. Millini, *Zeolites Catal.*, 2010, **2**, 449–491.
21 S. I. Zones, *Microporous Mesoporous Mater.*, 2011, **144**(1–3), 1–8.
22 U. Olsbye, S. Svelle, M. Bjørgen, P. Beato, T. V. W. Janssens, F. Joensen, S. Bordiga and K. P. Lillerud, *Angew. Chem., Int. Ed.*, 2012, **51**, 5810–5831.
23 S. T. Korhonen, D. W. Fickel, R. F. Lobo, B. M. Weckhuysen and A. M. Beale, *Chem. Commun.*, 2011, **47**, 800–802.
24 M. Moliner, C. Franch, E. Palomares, M. Grill and A. Corma, *Chem. Commun.*, 2012, **48**, 8264–8266.
25 P. J. Bereciartua, A. Cantín, A. Corma, J. L. Jordá, M. Palomino, F. Rey, S. Valencia, E. W. Corcoran Jr, P. Kortunov, P. I. Ravikovitch, A. Burton, C. Yoon, Y. Wang, C. Paur, J. Guzman, A. R. Bishop and G. L. Casty, *Science*, 2017, **358**, 1068–1071.
26 M. Dodin, J. L. Paillaud, Y. Lorgouillous, P. Caullet, E. Elkaim and N. Bats, *J. Am. Chem. Soc.*, 2010, **132**, 10221–10223.
27 J. L. Paillaud, B. Harbuzaru, J. Patarin and N. Bats, *Science*, 2004, **304**, 990–992.
28 Y. Lorgouilloux, M. Dodin, J. L. Paillaud, P. Caullet, L. Michelin, L. Josien, O. Ersen and N. Bats, *J. Solid State Chem.*, 2009, **182**, 622–629.
29 D. J. Earl, A. W. Burton, T. Rea, K. Ong, M. W. Deem, S. J. Hwang and S. I. Zones, *J. Phys. Chem. C*, 2008, **112**, 9099–9105.
30 L. Tang, L. Shi, C. Bonneau, J. Sun, H. Yue, A. Ojuva, B. L. Lee, M. Kritikos, R. G. Bell, Z. Bacsik, J. Mink and X. Zou, *Nat. Mater.*, 2008, **7**, 381–385.
31 A. Corma, M. T. Navarro, F. Rey, J. Rius and S. Valencia, *Angew. Chem., Int. Ed.*, 2001, **40**, 2277–2280.
32 Y. Yun, M. Hernandez, W. Wan, X. Zou, J. L. Jorda, A. Cantin, F. Rey and A. Corma, *Chem. Commun.*, 2015, **51**, 7602–7605.
33 J. Jiang, Y. Yun, X. Zou, J. L. Jorda and A. Corma, *Chem. Sci.*, 2015, **6**, 480–485.
34 M. Hernandez-Rodriguez, J. L. Jorda, F. Rey and A. Corma, *J. Am. Chem. Soc.*, 2012, **134**, 13232–13235.
35 J. Jiang, J. L. Jorda, M. J. Diaz-Cabañas, J. Yu and A. Corma, *Angew. Chem., Int. Ed.*, 2010, **49**, 4986–4988.
36 T. Blasco, A. Corma, M. J. Diaz-Cabanas, F. Rey, J. A. Vidal-Moya and C. M. Zicovich-Wilson, *J. Phys. Chem. B*, 2002, **106**, 2634–2642.
37 M. Moliner, T. Willhammar, W. Wan, J. Gonzalez, F. Rey, J. L. Jorda, X. Zou and A. Corma, *J. Am. Chem. Soc.*, 2012, **134**, 6473–6478.
38 A. Corma, M. J. Diaz-Cabanas, J. L. Jorda, F. Rey, G. Sastre and K. G. Strohmaier, *J. Am. Chem. Soc.*, 2008, **130**, 16482–16483.
39 A. Corma, M. J. Diaz-Cabanas, J. L. Jorda, C. Martinez and M. Moliner, *Nature*, 2006, **443**, 842–845.
40 J. Sun, C. Bonneau, A. Cantin, A. Corma, M. J. Diaz-Cabañas, M. Moliner, D. Zhang, M. Li and X. Zou, *Nature*, 2009, **458**, 1154–1157.
41 A. Corma, F. Rey, S. Valencia, J. L. Jorda and J. Rius, *Nat. Mater.*, 2003, **2**, 493–497.
42 P. E. Werner, L. Eriksson and M. Westdahl, *J. Appl. Crystallogr.*, 1985, **18**, 367–370.
43 J. Simancas, R. Simancas, P. J. Bereciartua, J. L. Jorda, F. Rey, A. Corma, S. Nicolopoulos, P. Pratim-Das, M. Gemmi and E. Mugnaioli, *J. Am. Chem. Soc.*, 2016, **138**, 10116–10119.
44 U. Kolb, E. Mugnaioli and T. E. Gorelik, *Cryst. Res. Technol.*, 2011, **46**, 542–554.
45 R. W. Grosse-Kuntstleve, L. B. McCusker and Ch. Baerlocher, *J. Appl. Crystallogr.*, 1999, **32**, 536–542.
46 R. Bialek, *KRIBER. Crystallographic computation program*, ETH Zurich Institut fur Kristallographie, Zurich, Switzerland, 1991.
47 Ch. Baerlocher, A. Hepp and W. M. Meier, *DLS-76. Distance least squares refinement program*, ETH Zurich Institut fur Kristallographie, Zurich, Switzerland, 1977.
48 F. Fauth, I. Peral, C. Popescu and M. Knapp, *Powder Diffr.*, 2013, **28**(S2), S360–S370.
49 I. Peral, J. McKinlay, M. Knapp and S. Ferrer, *J. Synchrotron Radiat.*, 2011, **18**, 1.
50 J. Rodríguez-Carvajal, *Commission on Powder Diffraction (IUCr) Newsletter*, 2001, **26**, 12.